ARTICLE

A Strong Integrated Strength and Toughness Artificial Nacre Based on Dopamine Cross-Linked Graphene Oxide

Wei Cui,[†,⊥] Mingzhu Li,[‡,⊥] Jiyang Liu,[†,⊥] Ben Wang,[§] Chuck Zhang,[§] Lei Jiang,[†] and Qunfeng Cheng[†,*]

[†]Key Laboratory of Bio-inspired Smart Interfacial Science and Technology of Ministry of Education, School of Chemistry and Environment, BeiHang University, Beijing 100191, P. R. China, [‡]Laboratory of New Materials, Institute of Chemistry, Chinese Academy of Science, Beijing 100190, P. R. China, and [§]School of Industrial and Systems Engineering, Georgia Institute of Technology, Atlanta, Georgia 30332, United States. [⊥]These three authors contributed equally to the work.

ABSTRACT Demands of the strong integrated materials have substantially increased across various industries. Inspired by the relationship of excellent integration of mechanical properties and hierarchical nano/microscale structure of the natural nacre, we have developed a strategy for fabricating the strong integrated artificial nacre based on graphene oxide (GO) sheets by dopamine cross-linking *via* evaporation-induced assembly process. The tensile strength and toughness simultaneously show 1.5 and 2 times higher than that of natural nacre. Meanwhile, the artificial nacre shows high electrical conductivity. This type of strong integrated artificial nacre has great potential applications in aerospace, flexible supercapacitor electrodes, artificial muscle, and tissue engineering.

KEYWORDS: artificial nacre · graphene oxide · bioinspired · integrated high performance · mechanical properties

Nacre, after billions of years of evolution, shows a unique integration of remarkable tensile strength and toughness,[1] which supplies a novel strategy for constructing the integrated high performance materials. A series of nacre-mimic layered materials with high mechanical properties have been successfully fabricated.[2−9] For example, Podsiadlo *et al.* shows the high tensile strength nacre-like layered materials through covalently cross-linking the nanoclay and the poly(vinyl alcohol) (PVA) composites but with lower toughness.[3] Studart *et al.* demonstrated the highest tough layered materials based on the platelets of Al_2O_3 and chitosan through the hydrogen bonding,[5] but the tensile strength shows a little lower. Bouville *et al.* demonstrated the highest stiffness bioinspired ceramics through the ice-templating.[8] Recently, the two-dimensional graphene oxide (GO) with rich functional groups on its surface, shows outstanding mechanical properties, which makes it to be one of the best candidates for fabricating the high performance layered materials.[10−17] For instance, a series of GO-based layered materials are fabricated including GO−poly(vinyl alcohol) (PVA),[18,19] GO−poly(methyl methacrylate) (PMMA),[18] GO−glutaraldehyde (GA),[20] GO−poly(acrylic acid) (PAA),[21] GO−borate,[22] GO−poly(ether imide) (PEI),[23] GO−10,12-pentacosadiyn-1-ol (PCDO),[24] and GO−silk fibroin (SL),[25,26] *etc.* However, only one kind of mechanical property, such as strength, stiffness, or toughness, has been improved. It is still a great challenge to simultaneously improve the strength and toughness. To solve this conflict between the strength, toughness, and stiffness and obtain the integrated materials,[27] two scientific problems should be considered. The first one is to build strong interfacial interaction between GO sheets,[28] for example, covalent cross-linking. The second one is the covalent cross-linking should be long chain between GO sheets, which can supply enough movement space for GO sheets when loading and absorb much more energy. The dopamine (DA), a mimic of the specialized mussel adhesive protein which contains both the functional catechol group and amine group,[29,30] is good choice, which can react

* Address correspondence to cheng@buaa.edu.cn.

Received for review July 9, 2014 and accepted August 8, 2014.

Published online August 08, 2014
10.1021/nn503755c

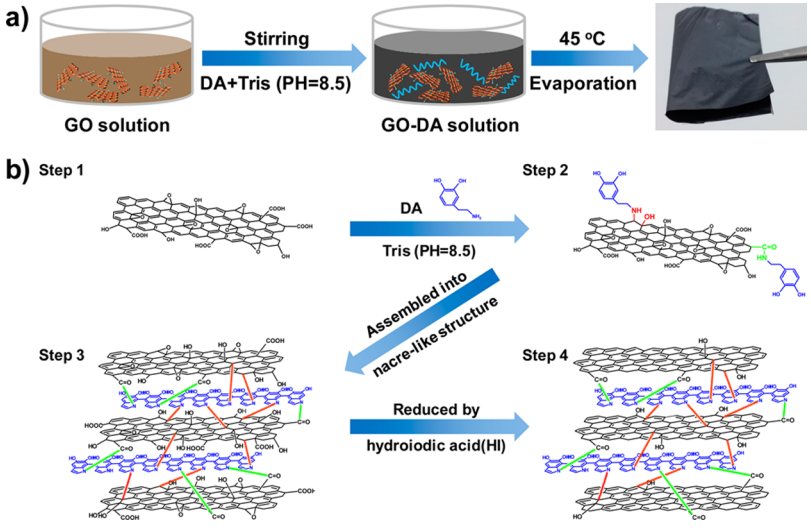

Scheme 1. Illustration of the preparation process of the artificial nacre. (a) The GO sheets were firstly dispersed into deionized (DI) water. Then, the Tris buffer solution (pH = 8.5) and DA was added. After the solution stirred for several minutes at room temperature, the color of mixture solution turned black from brown, and after a drying step in an oven at 45 °C, the artificial nacre based on GO was obtained. (b) The whole process of fabrication was divided into four steps. Step 1: the GO sheets were firstly dispersed in the DI water with brown color. Step 2: the reactions between GO sheets and DA molecules, and self-polymerization between DA molecules into poly(dopamine) (PDA), resulted in the color of solution turning black from brown. Step 3: the black solution was transferred into an oven and assembled into GO−PDA with nacre-like structure *via* evaporation. Step 4: the resultant GO−PDA composites were further reduced by hydroiodic acid (HI).

with GO sheets and self-polymerize into long chain polymers of poly(dopamine) (PDA).

Herein, the integrated artificial nacres are fabricated through evaporation-induced assembly process. The tensile strength and toughness simultaneously show 1.5 and 2 times higher than that of the natural nacre. Meanwhile, the resultant artificial nacre shows high electrical conductivity, which supplies great potential applications for the novel strong integrated artificial nacre in the fields of aerospace, flexible supercapacitor electrode, artificial muscle, and tissue engineering.

RESULTS AND DISCUSSION

The fabrication process of artificial nacre is shown in Scheme 1a. The GO sheets were first dispersed into deionized (DI) water. Then, the Tris buffer solution (pH = 8.5) and DA was added. After the solution stirred for several minutes at room temperature, the color of mixture solution turned black from brown, and after a drying period of about 2 days in an oven at 45 °C, the GO-based artificial nacre was obtained, which showed a little bit of metallic luster.[31] The whole process of fabrication was divided into four steps, as illustrated in Scheme 1b. In the step 1, the GO sheets first are dispersed in the DI water with brown color. In the step 2, the DA powder and Tris solution were added with continuous stirring in air. Chemical cross-linking reactions between GO and DA molecules, and self-polymerization between DA molecules into poly(dopamine) (PDA) under weak alkaline environment happened,[29] resulting in the color of solution turning black from brown. The adjacent GO sheets were cross-linked by the PDA. In the step 3, the black solution was transferred into an oven at 45 °C in air for about 2 days, then the black solution would be assembled into GO−PDA with nacre-like structure *via* slowly evaporation. To enhance the mechanical properties of the artificial nacre GO−PDA composites, the resultant GO−PDA composites were further reduced by hydroiodic acid (HI) in the step 4, as our previous report.[24]

Due to the great impact of matrix loading on the mechanical properties of resultant composites, we fabricated a series of GO−PDA composites. The DA content can be controlled in the evaporation-induced assembly process, and the exact content of PDA was determined using thermogravimetric analysis (TGA), as shown in Table 1 and Figure S1 in the Supporting Information. Fourier Transform infrared spectroscopy (FTIR) was conducted to verify the reaction between GO sheets and DA molecules, as shown in Figure 1a. The characteristic peak of carbonxyl groups on GO sheets with 1725 cm^{-1} almost disappears in the GO−PDA composites, and the epoxide characteristic peaks of 870 and 1220 cm^{-1} on the GO sheets also disappear in the GO−PDA composites, indicating the reaction between epoxide groups on GO and amine groups on DA. Moreover, the absorption peaks at 1590 and 1232 cm^{-1} in the GO−PDA composites, attributed to deformation vibration of −N−H bonding and stretching vibration of −C−N bonding, respectively, further confirm the reaction happening between epoxide groups on GO and amine groups on DA. Raman spectra were conducted as shown in the Figure 1b. The I_D/I_G ratio decreases from 1.5 for pure GO film to 1.29 for GO−PDA−VI composite, which indicates the reaction between GO and DA molecules in the

evaporation-induced self-assembly process, on the other hand, the I_D/I_G ratio of the physical blend of GO/PDA (95:5) composite is still as high as 1.47, showing no reaction between GO and PDA in the physical blend.

The X-ray photoelectron spectroscopy (XPS) was conducted to further verify the reaction between GO and DA, as shown in Figure 1c. A new strong peak of 285.8 ev appears in the GO—PDA—VI composites, which is attributed to the C—N bonding, indicating the grafting of DA on GO sheets, which is in consonance with the FTIR results. The DA is usually used as reductant of GO in the previous reports.[31] Herein, we further reduce the GO—PDA composite with HI, and the XPS spectra of rGO and rGO—PDA—VI are shown in Supporting Information Figure S2.

X-ray diffraction (XRD) results show that the interlayer distance of the GO—PDA composites increases with the loading of DA (Figure 1d), indicating that the PDA was successfully embedded into the GO sheets. The interlayer distance (*d*-spacing) of pure GO film is about 8.28 Å ($2\theta = 10.68°$), which is well consistent with the previous report.[10] The *d*-spacing of GO—PDA composites with different GO contents is listed in Supporting Information Table S1. For GO—PDA—I, the *d*-spacing is about 9.88 Å. The improvement of *d*-spacing shows a little bit of low relative to the addition of DA molecules. This is because the excess DA molecules are self-polymerized into PDA, and coated on the surface of GO. This can be confirmed by the cross-section morphology with SEM image as show in Supporting Information Figure S3. It is obvious that the higher the GO loading is, the better the layer structure will be.

TABLE 1. PDA Content and the Electrical Conductivity of Pure GO and GO—PDA Composites

			electrical conductivity ($S \cdot m^{-1}$)	
sample	input DA content [wt %]	PDA content by TGA	before HI reduction	after HI reduction
GO	0	0	2.7×10^{-2}	4480
GO—PDA—I	50	47.6	3.2×10^{-2}	70
GO—PDA—II	33	31.5	4.6×10^{-2}	440
GO—PDA—III	25	23.7	8.6×10^{-2}	890
GO—PDA—IV	20	18.9	0.92	1170
GO—PDA-V	10	8.9	1.7	2130
GO—PDA—VI	5	4.6	2.9	1850

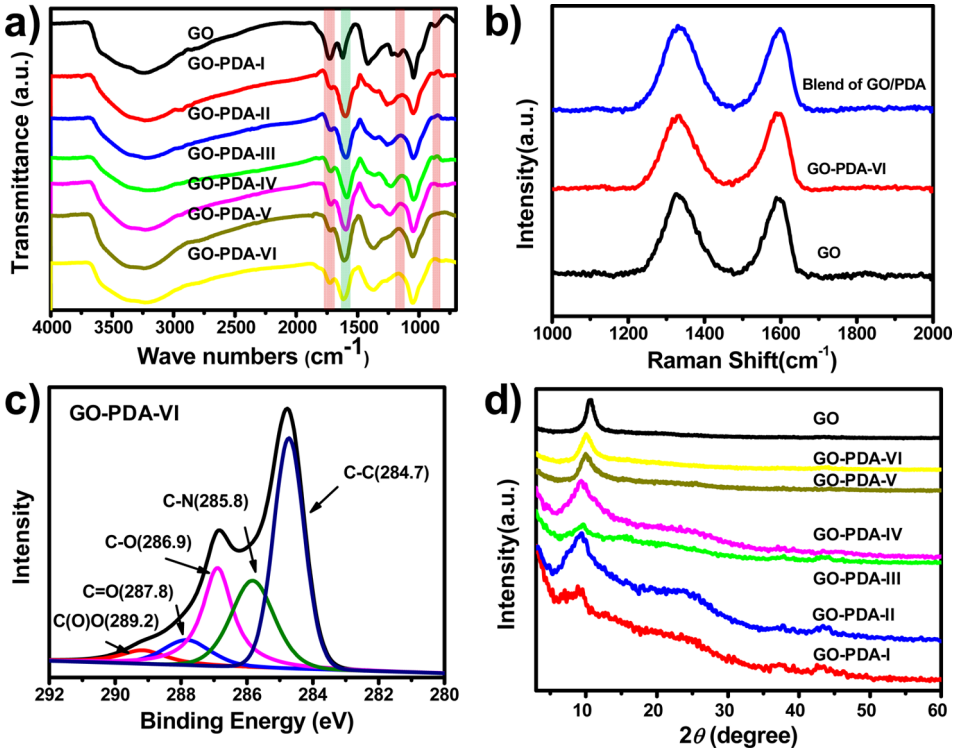

Figure 1. (a) FTIR spectra of pure GO films, GO—PDA composites with different content of PDA. Peaks at 1725 cm^{-1} of carboxyl group, 1220 and 870 cm^{-1} of epoxide groups in the GO—PDA composites disappear and the emerging of peak at 1590 cm^{-1} of —N—H bonding in the GO—PDA composites indicate the reaction between epoxide groups on GO sheets and amine groups on DA. (b) Raman spectra of GO film, GO—PDA—VI composites and physical blend of GO/PDA (95:5). The I_D/I_G ratio decreases from 1.5 for pure GO film to 1.29 for GO—PDA—VI composite, indicating the reaction between GO and DA molecules in the evaporation-induced self-assembly process. On the other hand, the I_D/I_G ratio of the physical blend of GO/PDA (95:5) composite is until as high as 1.47, showing no reaction between GO and PDA in the physical blend. (c) XPS spectrum of the GO—PDA—VI composites. The appearance of new peak of 285.8 eV, attributed to the C—N bonding, indicates the grafting of DA on GO sheets. (d) XRD of pure GO film, and the GO—PDA composites. The interlayer distance (*d*-spacing) of the GO—PDA composites increases with the content of DA, indicating that the PDA was successfully embedded into the GO sheets.

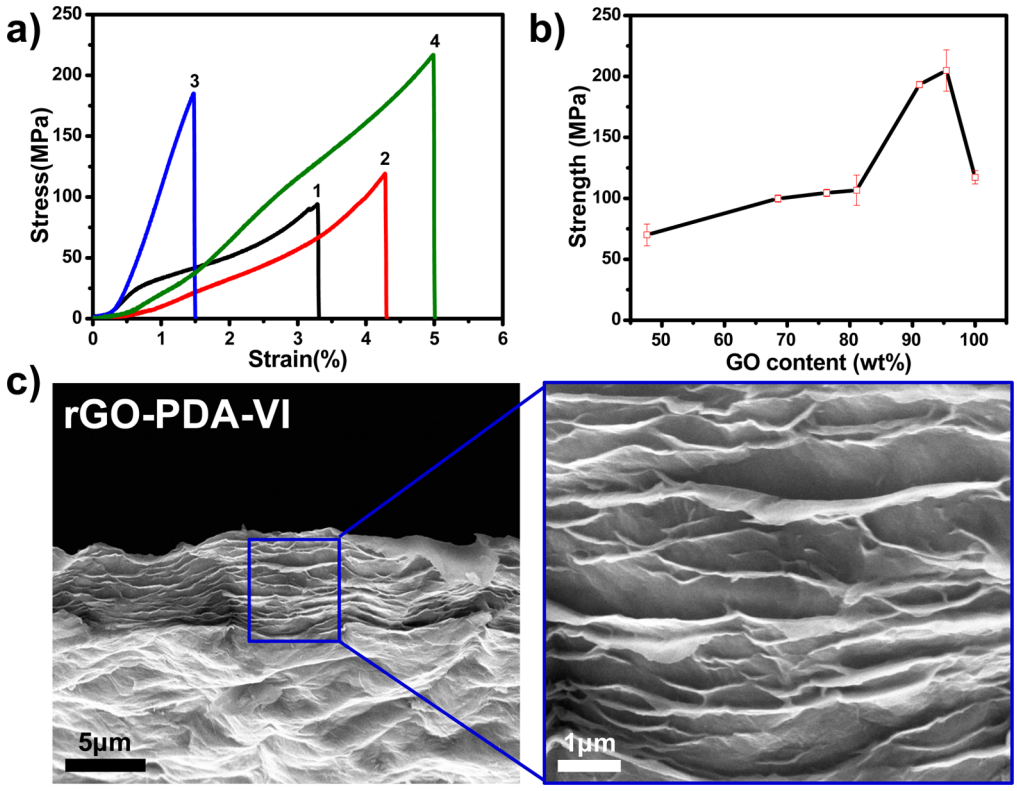

Figure 2. (a) Tensile stress−strain curves of GO film (Curve 1), rGO film (Curve 2), GO−PDA−VI (Curve 3), and rGO−PDA−VI composites (Curve 4). (b) The ultimate strength of rGO−PDA composites with different GO contents (wt %), indicating the tensile strength increases with the GO content. (c) Fracture surface morphology of the rGO−PDA−VI composites. The strong covalent cross-linking leads to curve of GO sheets in the rGO−PDA−VI composites.

The cross-section of the GO−PDA−I composite does not clearly show the layered structure, because the PDA is wrapped in the GO sheets. With increasing GO content, the *d*-spacing of GO−PDA composites decreases to 8.81 Å corresponding to the GO−PDA−VI composites.

In fact, the excess PDA acts as intercalating impurities, and may only increase the area of cross-section of GO−PDA composites, which reduces the mechanical properties of GO−PDA composites. The cross-section of the GO−PDA and rGO−PDA composites with different PDA contents is shown in Supporting Information Figure S3. The typical strain−stress curves of rGO−PDA composites were shown in Figure 2a. The tensile strength and toughness of the pure GO film are about 91.2 ± 1.6 MPa and 1.4 ± 0.1 MJ m^{-3}, respectively, which are well consistent with the previous reports.[21] After HI reduction, the tensile strength and toughness of rGO film increased to 117.3 ± 5.5 MPa and 1.7 ± 0.1 MJ m^{-3}. With increasing of the GO content in the resultant composites, the tensile strength of GO−PDA composites is dramatically enhanced, as shown in Figure 2b and the detailed mechanical properties are listed in Supporting Information Table S2.

For the rGO−PDA−VI composites, the PDA content is only about 4.6 wt % by TGA, which well fits the natural nacre with inorganic calcium carbonate content as much as 95 vol %.[1] It is in well accordance with the idea of bionics. The tensile strength of rGO−PDA−VI composite reaches up to 204.9 ± 17.0 MPa, and the toughness is as high as 4.0 ± 0.9 MJ·m^{-3}, which is simultaneously 1.5 and 2 times higher than that of natural nacre with 80−135 MPa and 1.8 MJ·m^{-3}, respectively,[32] indicating the integrated tensile strength and toughness properties. This is because of the effective covalent cross-linking between GO sheets and PDA. For comparison, a control sample of physical blend of GO and PDA with the ratio of 95:5 was made and tested, and the tensile strength is only 81.8 ± 10.6 MPa and the toughness is only 0.4 ± 0.1 MJ·m^{-3} as shown in Supporting Information Figure S4, which are lower than that of *in situ* polymerization of GO−PDA−VI composites, because of only the weak hydrogen bond between GO sheets and PDA.

The fracture morphology of the rGO−PDA−VI composites is shown in Figure 2c. Due to HI reduction, the excess functional groups on the GO sheets are removed, and the friction between adjacent rGO sheets is much higher, absorbing more energy in the fracture process. When loading is further increased, the chemical bonds of strong covalent cross-linking between GO sheets and PDA are broken, which simultaneously results in that the fracture edges of GO sheets turn to curve rather than straightness from the cross section, that is well consistent with our previous report.[24] The typical fracture morphology suggests when the cross-linking bonds in the rGO−PDA−VI composite break,

the slippage turns up between the GO sheets, just like adding lubrication on the layers to decrease interactive friction, which leads to slippage first, breakage second, then large deformation leads to curving of GO sheets. This unique intrinsic processing allows the rGO–PDA–VI composite to bear stronger force and shape greater deformation so that the rGO–PDA–VI composite with both high strength and toughness can be simultaneously obtained.

In our previous work, the tough artificial nacre based on GO sheets was demonstrated through covalent cross-linking the long chain molecule PCDO between GO sheets.[24] However, because the loading of PCDO cannot be further improved, it is difficult to improve the tensile strength of the artificial nacre with high toughness. Herein, the DA molecules not only react with GO sheets into strong covalent cross-linking, but also self-polymerize into long chain polymer of PDA, which can supply enough space for GO sheets slippage and absorb much more energy when loading. The tensile strength of the rGO–PDA–VI reaches 204.9 ± 17.0 MPa, corresponding to 58% improvement for the previous report of rGO–PCDO artificial nacre of 129.6 ± 18.5 MPa.[24] The toughness of the rGO–PDA–VI composites is up to 4.0 ± 0.9 MJ·m^{-3}, which is a little bit higher than that of the previous rGO–PCDO artificial nacre of 3.91 ± 0.03 MJ·m^{-3}.[24]

The advantage of this strategy for fabricating artificial nacre compared with natural nacre and other nacre-like materials based on GO sheets is shown in Figure 3. The other approaches for constructing the GO-based nacre-like materials always show improvement in only one kind of mechanical properties, such as tensile strength or stiffness or toughness. For example, An *et al.* constructed high stiff bioinspired GO layered materials through borate cross-linking inspired by the Maize plants.[22] The stiffness of borate cross-linked GO (GO–borate) sheets materials is as high as 127 ± 4 GPa. The dramatic increases are attributed to the covalent borate orthoester bonds between GO sheets and borate ions. On the other hand, the strain of GO–borate materials is only 0.15% and the toughness is as low as 0.14 MJ·m^{-3}, which is lower than one tenth of natural nacre (1.8 MJ·m^{-3}).[32] Tian *et al.* realized high tensile strength nacre-like materials through polyetherimide (PEI) cross-linking GO sheets (PGO–PEI).[23] The tensile strength reaches up 209.9 MPa. However, the elongation dramatically decrease into only 0.22% with significant increase of strength and modulus due to the connected interlayer interaction through cross-linking, and the toughness is only 0.23 MJ·m^{-3}, which is still only eighth of natural nacre (1.8 MJ·m^{-3}).[32] Recently, Hu *et al.* demonstrated the high tensile strength rGO-based materials with 300 MPa at low silk fibroin content (2.5%) (rGO–SL),[26] which may be caused by additional cross-linking and the reducing ability of silk backbones. However, the toughness is only 2.8 MJ·m^{-3}, which is lower than our previous report (3.91 MJ·m^{-3}).[24]

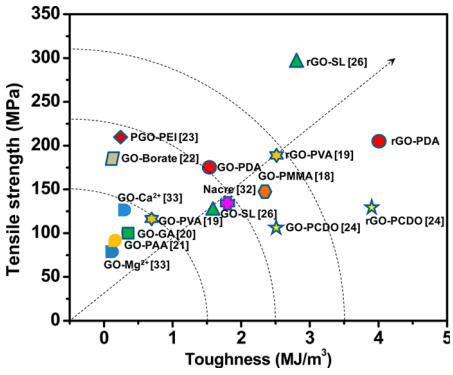

Figure 3. Comparison of tensile strength and toughness of our artificial nacre of the GO–PDA–VI and rGO–PDA–VI composites with the natural nacre, and other layered GO-based materials with different cross-linking strategies. The rGO–PDA–VI composite show the strong integrated strength and toughness compared with other layered materials based on GO, such as hydrogen interaction of GO–PVA, and GO–SL, ionic interaction of GO–Ca^{2+}, GO–Mg^{2+}, short chain covalent cross-linking of GO–GA, and PGO–PEI, and long chain covalent cross-linking of GO–PCDO.

The tensile strength of rGO–PDA–VI composites is comparable to GO–PEI and higher than GO–borate. The toughness of rGO–PDA–VI is 16- and 27-fold higher than PGO–PEI[23] and GO–borate,[22] respectively. Although the tensile strength is lower than rGO–SL,[26] however, the toughness is 43% higher than rGO–SL. This strategy for fabricating the GO-based composites is also superior to other approaches for constructing the GO-based layered materials, such as hydrogen interaction between GO sheets and matrix including GO-PMMA with strength of 148.3 MPa and toughness of 2.35 MJ·m^{-3},[18] rGO–PVA with strength of 188.9 MPa and toughness of 2.52 MJ·m^{-3},[19] and ion interaction between GO sheets and matrix, including GO–Mg^{2+}, GO–Ca^{2+} materials with strength of 80.6 and 125.8 MPa, and toughness of 0.13 and 0.31 MJ·m^{-3}, respectively,[33] and other covalent bonding including glutaraldehyde (GA) covalent cross-linking (GO–GA) with strength of 101 MPa and toughness of 0.3 MJ·m^{-3},[20] poly(acrylic acid) (PAA) cross-linking (GO–PAA) with strength of 91.9 MPa and toughness of 0.15 MJ·m^{-3}.[21] The detailed mechanical properties of our artificial nacre, natural nacre and other GO-based layered materials are listed in Supporting Information Table S3.

Due to the defects introduced in the process of chemical exfoliation, the graphene oxide film shows low conductivity of 2.7 × 10^{-2} S·m^{-1}. DA is green reduction agent for GO sheets,[31] resulting in the high electrical conductivity of GO–PDA composites than pure GO film, as listed in Table 1. For the GO–PDA–VI composites, the electrical conductivity reaches as high as 2.9 S·m^{-1}, which is 2 orders of magnitude higher than that of pure GO film. With the PDA loading increasing, the electrical conductivity of GO–PDA composites dramatically decrease to 3.2 × 10^{-2} S·m^{-1} for GO–PDA–I, because the PDA is nonconductive

material, excess PDA wrapped the GO layers and impaired the conductivity of GO–PDA composites. After HI reduction, the electrical conductivity of pure rGO film reaches 4480 $S \cdot m^{-1}$, which is well consistent with the previous reported value of 5000 $S \cdot m^{-1}$.[34] The artificial nacre of rGO–PDA–VI composite shows the electrical conductivity as high as 1850 $S \cdot m^{-1}$, which is a little higher than the previous reported rGO–SL (1350 $S \cdot m^{-1}$).[26]

CONCLUSION

Inspired by the natural nacre, we successfully fabricated the strong integrated artificial nacre based on dopamine cross-linked GO sheets. Compared with previous approaches, this cross-linking strategy effectively realized the integration of the high tensile strength and excellent toughness in the GO-based layered composites. Meanwhile, the artificial nacre shows high electrical conductivity. This study opens the door toward bioinspired production of the GO-based composites with integrated performance of high tensile strength and excellent toughness, showing great promising applications in aerospace, flexible supercapacitor electrodes, artificial muscles, and tissue engineering.

METHODS

Materials. Graphene oxide sheets were purchased from XianFeng NANO Co., Ltd. The density of GO was about 1.6–1.8 g/cm^3, which was consistent with the previous report.[10] The diameter of GO sheets was in the range of 1–5 μm, as shown in Figure S5 in the Supporting Information. The dopamine (DA), Tris(hydroxymethyl)aminomethane and 57 wt % HI were purchased from Sigma-Aldrich.

Fabrication of the GO–PDA Composites. Preparation of Tris buffer solution (pH = 8.5): 1.514 g of Tris solid powder was dissolved in 50 mL of deionized water. Then, 0.32 mL of hydrochloric acid (HCl) was added, and the solution was stirred for 10 min to obtain the uniform and transparent solution. Finally, 250 mL of deionized water was added, and the solution stirred for 10 min to obtain the Tris buffer solution with pH = 8.5. GO was dispersed in deionized water with stirring for about 1 h and ultrasonicating for 0.5 h into the transparent brown solution. Then, the Tris buffer solution (pH = 8.5) and DA were added, followed by continuous stirring for 24 h. The color of the mixing solution turned from brown to black. The mixing solution was poured into the glassware, and transferred into an oven with temperature of 45 °C. After 48 h of drying, the GO–PDA composites were obtained and removed from the glassware using diluted hydrofluoric acid (HF). The rGO–PDA composites were obtained through reduction by hydroiodic acid (HI). The oxidized iodine on the surface of rGO–PDA composites was cleaned out with ethanol washing for 4 days.

Characterization. Mechanical properties were tested by Shimadzu AGS-X Tester with gauge length of 5 mm, and loading rate of 1 mm min^{-1}. All the samples were cut into strips with the length of 20 mm and the width of 3 mm. Fourier transform infrared spectroscopy (FTIR) was conducted through a Thermo Nicolet nexus-470 instrument. X-ray photoelectron spectroscopy (XPS) was performed using ESCALab220i-XL (Thermo Scientific) with the X-ray source of a monochromatic Al Kα. X-ray diffraction (XRD) was collected from Shimadzu LabX XRD-6000. Raman spectroscopy was conducted using a LabRAM HR800 with 633 nm laser excitation. Scanning electron microscopy (SEM) images were obtained by Quanta 250 FEG and JSM-7500F. The thermogravimetric analysis (TGA) was performed on TG/DTA6300, NSK under argon with a temperature rising rate of 10 °C min^{-1}. The electrical conductivity of the composites was measured with the CHI660B electrochemical workstation.

Conflict of Interest: The authors declare no competing financial interest.

Acknowledgment. This work was supported by the National Research Fund for Fundamental Key Projects (2010CB934700), the National Natural Science Foundation of China (21273017, 51103004, 91127038), Program for New Century Excellent Talents in University (NCET-12-0034), Beijing Nova Program (Z121103002512020, Z131103000413051), Beijing Science and Technology Program (Z121100001312004), Fok Ying-Tong Education Foundation (141045), Open Project of Beijing National Laboratory for Molecular Sciences, the 111 Project (B14009), and the Fundamental Research Funds for the Central Universities (YWF-14-HXXY-018).

Supporting Information Available: TGA curves of PDA, GO, and GO–PDA composites; XPS spectra of rGO film and the rGO–PDA–VI composites; cross-section fracture morphology of the artificial nacre with different GO contents before and after HI reduction; stress–strain curve of physical blend of GO/PDA (95:5) composites; AFM image of GO sheets; tables of *d*-spacing and mechanical properties of the GO–PDA and rGO–PDA composites, and mechanical properties of the natural nacre, artificial nacre of the GO–PDA–VI and rGO–PDA–VI, and other GO-based layered materials. This material is available free of charge *via* the Internet at http://pubs.acs.org.

REFERENCES AND NOTES

1. Jackson, A.; Vincent, J.; Turner, R. The Mechanical Design of Nacre. *Proc. R. Soc. London, Ser. B* **1988**, *234*, 415–440.
2. Tang, Z.; Kotov, N. A.; Magonov, S.; Ozturk, B. Nanostructured Artificial Nacre. *Nat. Mater.* **2003**, *2*, 413–418.
3. Podsiadlo, P.; Kaushik, A. K.; Arruda, E. M.; Waas, A. M.; Shim, B. S.; Xu, J. D.; Nandivada, H.; Pumplin, B. G.; Lahann, J.; Ramamoorthy, A.; *et al.* Ultrastrong and Stiff Layered Polymer Nanocomposites. *Science* **2007**, *318*, 80–83.
4. Munch, E.; Launey, M. E.; Alsem, D. H.; Saiz, E.; Tomsia, A. P.; Ritchie, R. O. Tough, Bio-Inspired Hybrid Materials. *Science* **2008**, *322*, 1516–1520.
5. Studart, A. R.; Bonderer, L. J.; Gauckler, L. J. Bioinspired Design and Assembly of Platelet Reinforced Polymer Films. *Science* **2008**, *319*, 1069–1073.
6. Yao, H.-B.; Tan, Z.-H.; Fang, H.-Y.; Yu, S.-H. Artificial Nacre-like Bionanocomposite Films from the Self-Assembly of Chitosan–Montmorillonite Hybrid Building Blocks. *Angew. Chem., Int. Ed.* **2010**, *49*, 10127–10131.
7. Cheng, Q.; Li, M.; Jiang, L.; Tang, Z. Bioinspired Layered Composites Based on Flattened Double-Walled Carbon Nanotubes. *Adv. Mater.* **2012**, *24*, 1838–1843.
8. Bouville, F.; Maire, E.; Meille, S.; Van de Moortele, B.; Stevenson, A. J.; Deville, S. Strong, Tough and Stiff Bioinspired Ceramics From Brittle Constituents. *Nat. Mater.* **2014**, *13*, 508–514.
9. Wang, J.; Cheng, Q.; Lin, L.; Jiang, L. Synergistic Toughening of Bioinspired Poly(vinyl alcohol)–Clay–Nanofibrillar Cellulose Artificial Nacre. *ACS Nano* **2014**, *8*, 2739–2745.
10. Dikin, D. A.; Stankovich, S.; Zimney, E. J.; Piner, R. D.; Dommett, G. H.; Evmenenko, G.; Nguyen, S. T.; Ruoff, R. S. Preparation and Characterization of Graphene Oxide Paper. *Nature* **2007**, *448*, 457–460.
11. Li, D.; Kaner, R. B. Graphene-Based Materials. *Science* **2008**, *320*, 1170–1171.

12. Bai, H.; Li, C.; Shi, G. Q. Functional Composite Materials Based on Chemically Converted Graphene. *Adv. Mater.* **2011**, *23*, 1089–1115.
13. Huang, X.; Qi, X.; Boey, F.; Zhang, H. Graphene-Based Composites. *Chem. Soc. Rev.* **2012**, *41*, 666–686.
14. Yang, M.; Hou, Y.; Kotov, N. A. Graphene-Based Multilayers: Critical Evaluation of Materials Assembly Techniques. *Nano Today* **2012**, *7*, 430–447.
15. Yang, X. W.; Cheng, C.; Wang, Y. F.; Qiu, L.; Li, D. Liquid-Mediated Dense Integration of Graphene Materials for Compact Capacitive Energy Storage. *Science* **2013**, *341*, 534–537.
16. Yang, Z.; Liu, M.; Zhang, C.; Tjiu, W. W.; Liu, T.; Peng, H. Carbon Nanotubes Bridged with Graphene Nanoribbons and Their Use in High-Efficiency Dye-Sensitized Solar Cells. *Angew. Chem., Int. Ed.* **2013**, *52*, 3996–3999.
17. Zhu, J.; Zhang, H. N.; Kotov, N. A. Thermodynamic and Structural Insights into Nanocomposites Engineering by Comparing Two Materials Assembly Techniques for Graphene. *ACS Nano* **2013**, *7*, 4818–4829.
18. Putz, K. W.; Compton, O. C.; Palmeri, M. J.; Nguyen, S. T.; Brinson, L. C. High-Nanofiller-Content Graphene Oxide–Polymer Nanocomposites *via* Vacuum-Assisted Self-Assembly. *Adv. Funct. Mater.* **2010**, *20*, 3322–3329.
19. Li, Y.-Q.; Yu, T.; Yang, T.-Y.; Zheng, L.-X.; Liao, K. Bio-Inspired Nacre-like Composite Films Based on Graphene with Superior Mechanical, Electrical, and Biocompatible Properties. *Adv. Mater.* **2012**, *24*, 3426–3431.
20. Gao, Y.; Liu, L.-Q.; Zu, S.-Z.; Peng, K.; Zhou, D.; Han, B.-H.; Zhang, Z. The Effect of Interlayer Adhesion on The Mechanical Behaviors of Macroscopic Graphene Oxide Papers. *ACS Nano* **2011**, *5*, 2134–2141.
21. Park, S.; Dikin, D. A.; Nguyen, S. T.; Ruoff, R. S. Graphene Oxide Sheets Chemically Cross-Linked by Polyallylamine. *J. Phys. Chem. C* **2009**, *113*, 15801–15804.
22. An, Z.; Compton, O. C.; Putz, K. W.; Brinson, L. C.; Nguyen, S. T. Bio-Inspired Borate Cross-Linking in Ultra-Stiff Graphene Oxide Thin Films. *Adv. Mater.* **2011**, *23*, 3842–3846.
23. Tian, Y.; Cao, Y. W.; Wang, Y.; Yang, W. L.; Feng, J. C. Realizing Ultrahigh Modulus and High Strength of Macroscopic Graphene Oxide Papers Through Crosslinking of Mussel-Inspired Polymers. *Adv. Mater.* **2013**, *25*, 2980–2983.
24. Cheng, Q.; Wu, M.; Li, M.; Jiang, L.; Tang, Z. Ultratough Artificial Nacre Based on Conjugated Cross-Linked Graphene Oxide. *Angew. Chem., Int. Ed.* **2013**, *52*, 3750–3755.
25. Hu, K.; Gupta, M. K.; Kulkarni, D. D.; Tsukruk, V. V. Ultra-Robust Graphene Oxide-Silk Fibroin Nanocomposite Membranes. *Adv. Mater.* **2013**, *25*, 2301–2307.
26. Hu, K. S.; Tolentino, L. S.; Kulkarni, D. D.; Ye, C. H.; Kumar, S.; Tsukruk, V. V. Written-in Conductive Patterns on Robust Graphene Oxide Biopaper by Electrochemical Microstamping. *Angew. Chem., Int. Ed.* **2013**, *52*, 13784–13788.
27. Ritchie, R. O. The Conflicts Between Strength and Toughness. *Nat. Mater.* **2011**, *10*, 817–822.
28. Cheng, Q.; Jiang, L.; Tang, Z. Bioinspired Layered Materials with Superior Mechanical Performance. *Acc. Chem. Res.* **2014**, *47*, 1256–1266.
29. Lee, H.; Dellatore, S. M.; Miller, W. M.; Messersmith, P. B. Mussel-Inspired Surface Chemistry for Multifunctional Coatings. *Science* **2007**, *318*, 426–430.
30. Lee, B. P.; Messersmith, P. B.; Israelachvili, J. N.; Waite, J. H. Mussel-Inspired Adhesives and Coatings. *Annu. Rev. Mater. Res.* **2011**, *41*, 99–132.
31. Xu, L. Q.; Yang, W. J.; Neoh, K.-G.; Kang, E.-T.; Fu, G. D. Dopamine-Induced Reduction and Functionalization of Graphene Oxide Nanosheets. *Macromolecules* **2010**, *43*, 8336–8339.
32. Wang, R. Z.; Suo, Z.; Evans, A. G.; Yao, N.; Aksay, I. A. Deformation Mechanisms in Nacre. *J. Mater. Res.* **2001**, *16*, 2485–2493.
33. Park, S.; Lee, K. S.; Bozoklu, G.; Cai, W.; Nguyen, S. T.; Ruoff', R. S. Graphene Oxide Papers Modified by Divalent Ions-Enhancing Mechanical Properties *via* Chemical Cross-Linking. *ACS Nano* **2008**, *2*, 572–578.
34. Chen, H.; Müller, M. B.; Gilmore, K. J.; Wallace, G. G.; Li, D. Mechanically Strong, Electrically Conductive, and Biocompatible Graphene Paper. *Adv. Mater.* **2008**, *20*, 3557–3561.